Impact-parameter dependence of the nuclear modification of J/ψ production in d+Au collisions at sqrt[s_{NN}]=200 GeV

D. McGlinchey, A. D. Frawley, and R. Vogt

Phys. Rev. C **87**, 054910 — Published 30 May 2013

DOI: 10.1103/PhysRevC.87.054910

Impact parameter dependence of the nuclear modification of J/ψ production in d+Au collisions at $\sqrt{s_{NN}} = 200$ GeV

D. McGlinchey,[1] A. D. Frawley,[1] and R. Vogt[2,3]

[1]*Physics Department, Florida State University, Tallahassee, FL 32306, USA**
[2]*Physics Division, Lawrence Livermore National Laboratory, Livermore, CA 94551, USA*
[3]*Physics Department, University of California at Davis, Davis, CA 95616, USA*

The centrality dependence of $\sqrt{s_{NN}} = 200$ GeV d+Au J/ψ data, measured in 12 rapidity bins that span $-2.2 < y < 2.4$, has been fitted using a model containing an effective absorption cross section combined with EPS09 NLO shadowing. The centrality dependence of the shadowing contribution was allowed to vary nonlinearly, employing a variety of assumptions, in an effort to explore the limits of what can be determined from the data. The impact parameter dependencies of the effective absorption cross section and the shadowing parameterization are sufficiently distinct to be determined separately. It is found that the onset of shadowing is a highly nonlinear function of impact parameter. The mid and backward rapidity absorption cross sections are compared with lower energy data and, for times of 0.05 fm/c or greater, data over a broad range of collision energies and rapidities are well described by a model in which the absorption cross section depends only on time spent in the nucleus.

PACS numbers: 25.75.Dw

I. INTRODUCTION

The modification of the gluon distributions in nuclear targets in high energy collisions, referred to here as gluon shadowing, is inherently interesting because of what it can teach us about the behavior of gluons at low Bjorken momentum fraction, x, where the gluon densities are high and saturation effects are expected to become important [1]. In addition, the modification of parton distributions in nuclei determines the initial conditions in a high energy nuclear collision. The initial conditions must be sufficently well understood before final-state hot matter effects can be isolated.

Parameterizations of the dependence of nuclear-modified parton distribution functions (nPDFs) on x and squared momentum transfer, Q^2, have been extracted by several groups from data that include deep inelastic electron-nucleus scattering (DIS) and Drell-Yan (DY) dilepton production in $p + A$ collisions. The DIS and DY data together provide strong constraints on valence and sea quark modifications [2–5]. Including neutrino-induced DIS data from heavy targets can discriminate between quarks and antiquarks [3, 4]. Inclusive pion production data from RHIC have also been incorporated to better constrain the gluon modifications [4, 5].

The measurements used to extract the nPDFs cited above [2–5] were all averaged over impact parameter. Therefore these nPDFs represent the parton modification averaged over the entire nucleus. If the modification of these nPDFs is desired as a function of the impact parameter, a specific dependence has been assumed [6]. A different approach, employing Gribov theory and incorporating diffractive data, allows the spatial information to be retained [7].

Recently, the impact parameter dependence of the EPS09 [5] and EKS98 [8] nPDFs has been parameterized [9] using the target mass dependence of the EPS09 and EKS98 parameter sets themselves. Terms up to fourth order in the nuclear thickness were necessary to produce A-independent coefficients.

In this paper, we address the impact parameter dependence of gluon shadowing in a different way, using the collision centrality and rapidity dependence of the J/ψ yields measured in $\sqrt{s_{NN}} = 200$ GeV d+Au collisions at RHIC [10]. We were motivated by the observation [10, 11] that the onset of J/ψ suppression at forward rapidity suggests a quadratic or higher dependence on the nuclear thickness function at impact parameter r_T, $T_A(r_T)$.

Gluon-gluon interactions dominate J/ψ production in high-energy hadronic collisions. Therefore, J/ψ production in p(d)+A collisions must reflect the gluon modification in the nuclear target. However, the measured modifications of J/ψ yields in p(d)+A collisions relative to $p + p$ collisions are also sensitive to the breakup of bound $c\bar{c}$ pairs by collisions with nucleons as the pairs pass through the medium. This effect, as well as effects due to any processes aside from shadowing, are usually parameterized by an effective absorption cross section, $\sigma_{\rm abs}$, fitted to the measured data (see *e.g.* Ref. [12]). The main goal of this work is to determine whether the impact parameter dependence of shadowing could be separated from the effects embodied in $\sigma_{\rm abs}$. Because the magnitude of the effect due to $\sigma_{\rm abs}$ depends exponentially on nuclear thickness for a constant $\sigma_{\rm abs}$, such separation may be possible if shadowing has a stronger thickness dependence than absorption.

*Electronic address: dmcglinchey@fsu.edu; Electronic address: afrawley@fsu.edu

II. MODEL INPUTS AND FITTING PROCEDURE

We assume that the shadowing modification, integrated over all r_T, could be described by the EPS09 NLO gluon modification [5] and fit both the r_T dependence of shadowing and the magnitude of $\sigma_{\rm abs}$ to the data. We tested two assumed forms for the r_T dependence of shadowing. Each of the two postulated behaviors had one or two parameters that were adjusted to the data, along with the magnitude of $\sigma_{\rm abs}$. A Glauber Monte Carlo calculation [13] was employed to compare the modification of the J/ψ yields to the PHENIX d+Au data, which are averaged over four centrality bins and twelve rapidity bins and then integrated over all p_T.

The Glauber Monte Carlo calculation allows the modification, calculated for individual nucleon-nucleus collisions, to be correctly averaged and integrated over collision centrality (related to impact parameter), rapidity and p_T. It also accounts for the effects of trigger efficiency in peripheral events. The Glauber parameters used here are identical to those used by PHENIX when calculating the experimental centrality distributions [10]. For that reason, we found we could drop the uncertainties from the measured data points that are associated with the mean number of binary collisions because they are common to both the data and the calculations. The Woods-Saxon nuclear density distribution has a radius of 6.34 fm and a diffuseness of 0.54 fm. It is assumed that the nuclear modification of the deuteron is negligible. The baseline J/ψ p_T and rapidity distributions used in the calculation were the $p+p$ distributions measured by PHENIX [14].

The values of the target momentum fraction, x_2, and squared momentum transfer, Q^2, were assumed to obey approximate $2 \rightarrow 1$ kinematics as functions of J/ψ rapidity and transverse momentum:

$$x_2 = \frac{\sqrt{M^2+p_T^2}}{\sqrt{s_{NN}}} e^{-y} \ , \quad Q^2 = M^2 + p_T^2 \ , \qquad (1)$$

where M is the J/ψ mass. The $2 \rightarrow 1$ kinematics are not strictly correct since a high p_T J/ψ requires production of an associated hard parton. However, Eq. (1) differs from exact $2 \rightarrow 1$ kinematics since the p_T of the J/ψ is finite. This approximation is close to the inclusive J/ψ kinematics in the color evaporation model (CEM) calculation described in Ref. [15], NLO in the total cross section. Thus the modifications of the gluon distribution in the nucleus are similar in the CEM calculation and the Glauber Monte Carlo using Eq. (1). This is demonstrated in Fig. 1, where the EPS09 NLO gluon modifications obtained from Eq. (1) are compared with those obtained from the CEM calculation. The results also agree with those found using PYTHIA [11].

We fitted $\sigma_{\rm abs}$ and the parameters derived from the r_T dependence of shadowing to the PHENIX data using a modified $\overline{\chi}^2$ function that properly accounts for all of the

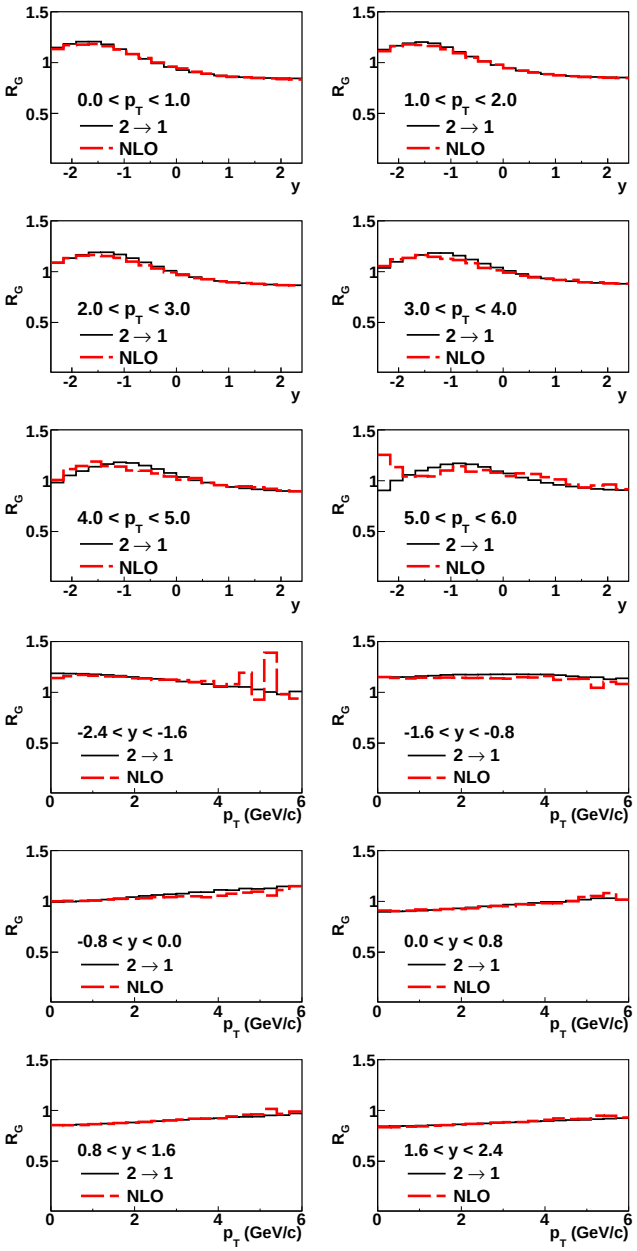

FIG. 1: (Color online) Comparison of the gluon modification as a function of rapidity and p_T obtained from EPS09 NLO using x and Q^2 values from Eq. (1) and from the CEM calculation [15], NLO in the total cross section.

experimental uncertainties [16]:

$$\overline{\chi}^2 = \left(\sum_{i=1}^{k} \frac{[R_{{\rm dAu}i} + \epsilon_{{\rm B}_i}\sigma_{{\rm B}_i} + \epsilon_{\rm C}\sigma_{{\rm C}_i} - R_{{\rm dAu}i}(M_{\rm shad}, \sigma_{\rm abs})]^2}{\overline{\sigma}_{{\rm A}_i}}\right) + {\epsilon_{\rm B}}^2 + {\epsilon_{\rm s}}^2 + {\epsilon_{\rm C}}^2, \qquad (2)$$

$$\overline{\sigma}_{{\rm A}_i} = \sigma_{{\rm A}_i} \left(\frac{R_{{\rm dAu}i} + \epsilon_{{\rm B}_i}\sigma_{{\rm B}_i} + \epsilon_{\rm C}\sigma_{{\rm C}_i}}{R_{{\rm dAu}i}} \right), \qquad (3)$$

$$\epsilon_{\mathrm{B}_i} = \epsilon_{\mathrm{B}} + \epsilon_{\mathrm{s}} \left(1 - 2 \frac{\langle \Lambda(r_T) \rangle_i - \langle \Lambda(r_T) \rangle_1}{\langle \Lambda(r_T) \rangle_k - \langle \Lambda(r_T) \rangle_1} \right), \quad (4)$$

where i is the index of the centrality bin, k is the number of centrality bins, $R_{\mathrm{dAu}i}$ is the data point, $R_{\mathrm{dAu}i}(M_{\mathrm{shad}}, \sigma_{\mathrm{abs}})$ is the model calculation for the trial values of the absorption cross section and shadowing prescription, $\sigma_{\mathrm{A}_i(\mathrm{B}_i,\mathrm{C}_i)}$ are the type A (point to point), B (correlated systematic), and C (global) uncertainties on the data point. The effect of systematic uncertainties is included by moving the data points through $\pm 3\sigma$ in the type B and type C uncertainties, while taking an appropriate $\overline{\chi}^2$ penalty. For each trial, $\epsilon_{\mathrm{B(C)}}$ is the fraction of one standard deviation by which the data point moves. Note that Eq. (4) contains a term that allows for some anti-correlation in the type B uncertainties. Here we allow the type B uncertainties to be linearly correlated about the center of the distribution, *i.e.* $+\epsilon_s$ in the first point and $-\epsilon_s$ in the last, and include a corresponding penalty for this correlation. The value of ϵ_s was varied in the range $\pm 3\epsilon_B$. Although this is a reasonable prescription, the amount of correlation in the type B uncertainty is unknown and could vary. However the type B uncertainty is small ($\sim 2\%$) and therefore any correlation should have a negligible effect on the end result when compared to the type A and C uncertainties.

Individual parameter uncertainties were evaluated by finding the values at which $\overline{\chi}^2$ increased by 1.0 with all other parameters re-optimized.

To begin, we assume that the shadowing strength is proportional to the nuclear thickness at impact parameter r_T raised to a power n, $T_A^n(r_T)$,

$$M_{\mathrm{shad}} = 1 - (1 - R_g(x, Q^2)) \left(\frac{T_A^n(r_T)}{a(n)} \right). \quad (5)$$

Here $R_g(x, Q^2)$ is the EPS09 NLO gluon modification and the normalization factor, $a(n)$, is adjusted so that the integral over all impact parameters returns the average EPS09 modification. The power n was allowed to be unphysically large, $n \leq 50$, while the modification was constrained to be positive. By allowing such arbitrarily large values of n, we can test the sensitivity of the data to the centrality dependence of the shadowing.

The results of fitting with Eq. (5), described in the next section, suggested that using a step function onset of shadowing, including a radius, R, and a diffuseness, d, parameter,

$$M_{\mathrm{shad}} = 1 - \left(\frac{1 - R_g(x, Q^2)}{a(R, d)(1 + \exp((r_T - R)/d))} \right). \quad (6)$$

would be more appropriate. Again, the normalization factor $a(R, d)$ is adjusted so that the integral over all impact parameters returns the average EPS09 modification. Thus, Eq. (6) was the second form of the r_T dependence of shadowing assumed in this work.

III. FITTING RESULTS

As a first step, the fits using Eq. (5) were made by determining the values of both σ_{abs} and n completely independently at each rapidity. This first step is not quite realistic because it ignores the correlations among some of the systematic uncertainties within each of the three spectrometer arms. However it provides an indication of how the centrality dependence varies with rapidity. The $\overline{\chi}^2$ contours in σ_{abs} and n corresponding to $\Delta\overline{\chi}^2 = 1.0$ and 2.3 are shown in Fig. 2 for the most backward rapidity, midrapidity, and the most forward rapidity. At midrapidity, the fits are insensitive to n because the shadowing effects are weak. At the most forward and backward rapidities the optimum n is large, $n \geq 10$, indicating that the data require a strongly nonlinear onset of shadowing or antishadowing as a function of impact parameter. Additionally, there is relatively little correlation, and thus little ambiguity, between n and σ_{abs} for n greater than a few.

The optimum value of σ_{abs} and the corresponding uncertainty at each rapidity is shown by the red squares in Fig. 3. The σ_{abs} values are reasonably well defined, with a minimum near midrapidity. Because the data at

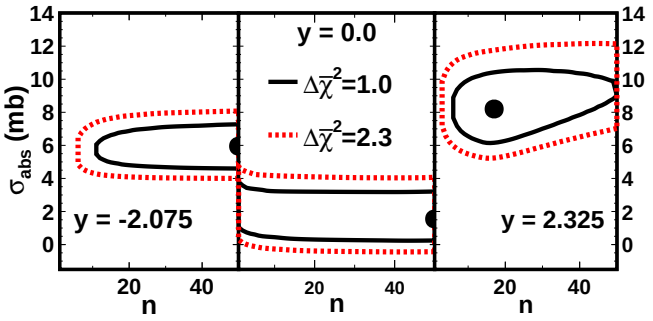

FIG. 2: (Color online) The $\overline{\chi}^2$ distributions for the most backward, mid and most forward rapidities when σ_{abs} and n are optimized separately at each rapidity.

all rapidities are consistent with $n \geq 5$, we repeated the fit assuming a rapidity-independent value of n. For this global fit, as well as for the one discussed later, the systematic uncertainties correlated within each experimental arm were handled correctly by being forced to move together. The optimum global power was $n = 15^{+5}_{-4}$. The $\overline{\chi}^2$/dof was 1.94 overall. The best fit values of σ_{abs} with $n = 15$ are shown as stars in Fig. 3.

The fits favor (or, at midrapidity, are consistent with) a shadowing modification that is negligible at large r_T but turns on sharply as r_T decreases below $\sim 2 - 3$ fm. This behavior suggested that the step function onset of shadowing described by Eq. (6) would be more appropriate.

For fits employing Eq. (6), we also initially fit the parameters R and d, along with σ_{abs}, independently at each rapidity. The optimum σ_{abs} values, the triangles in Fig. 3, are very similar to those obtained from the

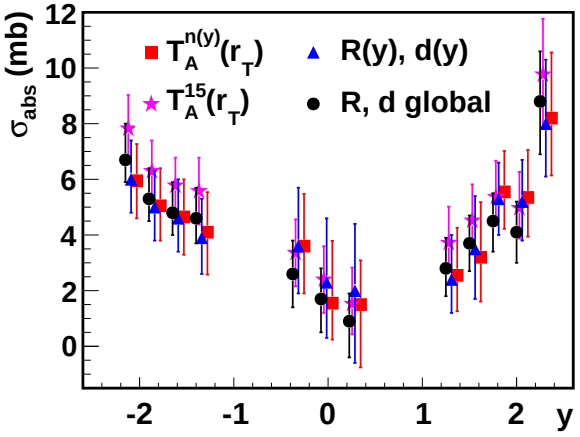

FIG. 3: (Color online) The optimum values of and uncertainties on $\sigma_{\rm abs}$ as a function of rapidity obtained from the four fits described in the text. For clarity, the rapidities for each fit are slightly offset.

earlier fits employing $T_A^n(r_T)$. The fits favor R values of about half the Au radius, $R \leq 3.5$ fm. While they also favor a small diffuseness parameter, they are relatively insensitive to the value of d.

Finally, we fit $\sigma_{\rm abs}$ at each rapidity while requiring a global fit to the values of R and d. The $\overline{\chi}^2$/dof was 1.96 over all values of y. The best fit $\sigma_{\rm abs}$ at each rapidity are shown as circles in Fig. 3. The $\overline{\chi}^2$ contours in R and d are shown in Fig. 4. The optimum global parameter values are $R = 2.4^{+0.53}_{-0.85}$ fm and $d = 0.12^{+0.52}_{-0.10}$ fm, where the uncertainties are obtained from the maximum extent of the $\Delta\overline{\chi}^2 = 1.0$ contour. The fit results are compared with

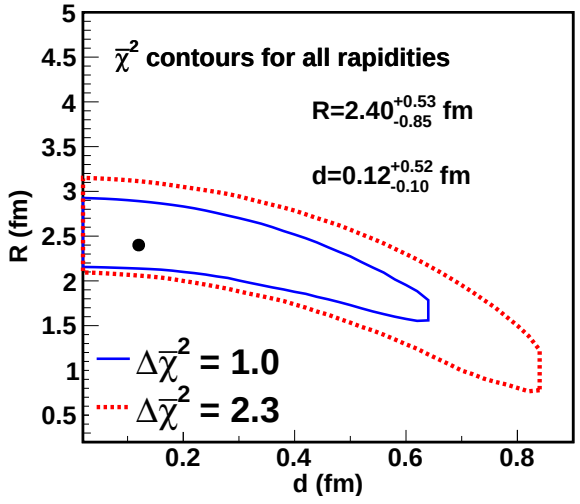

FIG. 4: (Color online) The $\overline{\chi}^2$ contours obtained from the fits with global values of R and d, Eq. (6). The uncertainties in R and d are taken from the maximum extent of the $\Delta\overline{\chi}^2 = 1$ contour.

the measured $R_{\rm dAu}$ as a function of r_T in Fig. 5 where the mean r_T values are the averages obtained from the Glauber model for the four PHENIX centrality bins. The dashed curves indicate the uncertainty in $R_{\rm dAu}$ due to the uncertainty in $\sigma_{\rm abs}$. Because $\overline{\chi}^2$ includes the global uncertainties on the data, the best fit values may be slightly vertically offset in order to achieve the best overall $\overline{\chi}^2$.

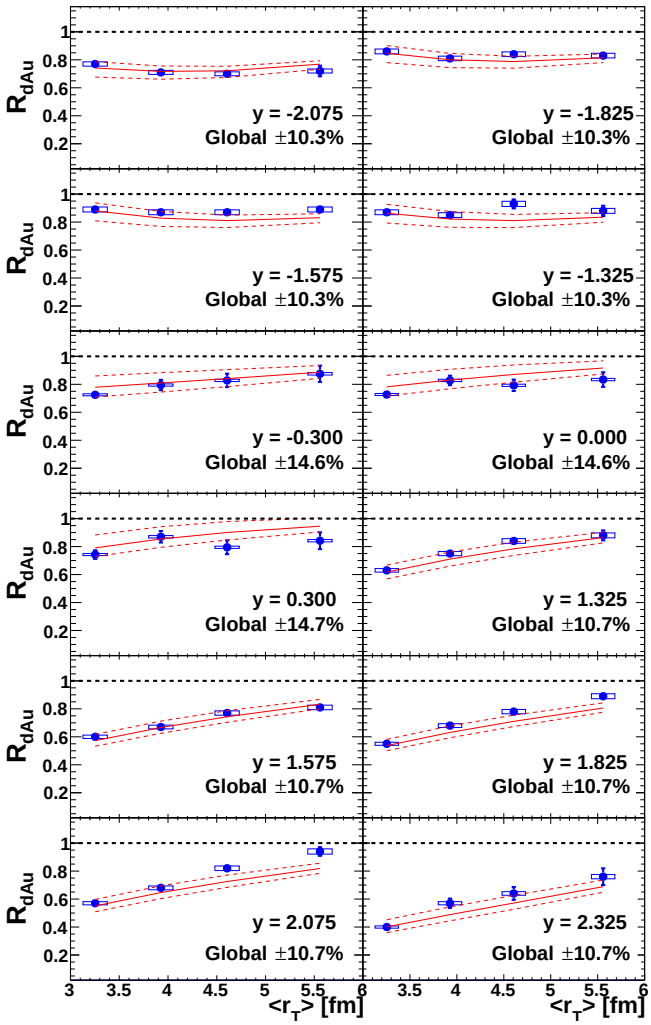

FIG. 5: (Color online) Comparison to the data of the best fits with global R and d values.

IV. DISCUSSION OF RESULTS

This study indicates that, due to their very different r_T dependence, there is little ambiguity between modifications due to shadowing and the effective absorption cross section $\sigma_{\rm abs}$. For perspective, we first compare the modifications due to shadowing and the effective absorption cross section calculated from our fit parameters. Then we discuss the results for effective absorption and shadowing, which presumably reflect different physics processes, separately.

A. Relative contributions of shadowing and absorption

It is of interest to contrast the modifications due to shadowing with those due to the effective absorption cross section. This is done in Fig. 6, after averaging over the PHENIX centrality resolution.

We find that the nuclear modification due to the effective absorption cross section is typically larger than that due to shadowing ($R_{\rm dAu}$ is smaller), even at forward and backward rapidities, where shadowing effects are strongest. However, the r_T dependence is stronger for shadowing and the overall r_T dependence of $R_{\rm dAu}$ more closely follows that for shadowing alone except at $y = -0.3$ where $R_{\rm dAu} \sim 1$ due to shadowing.

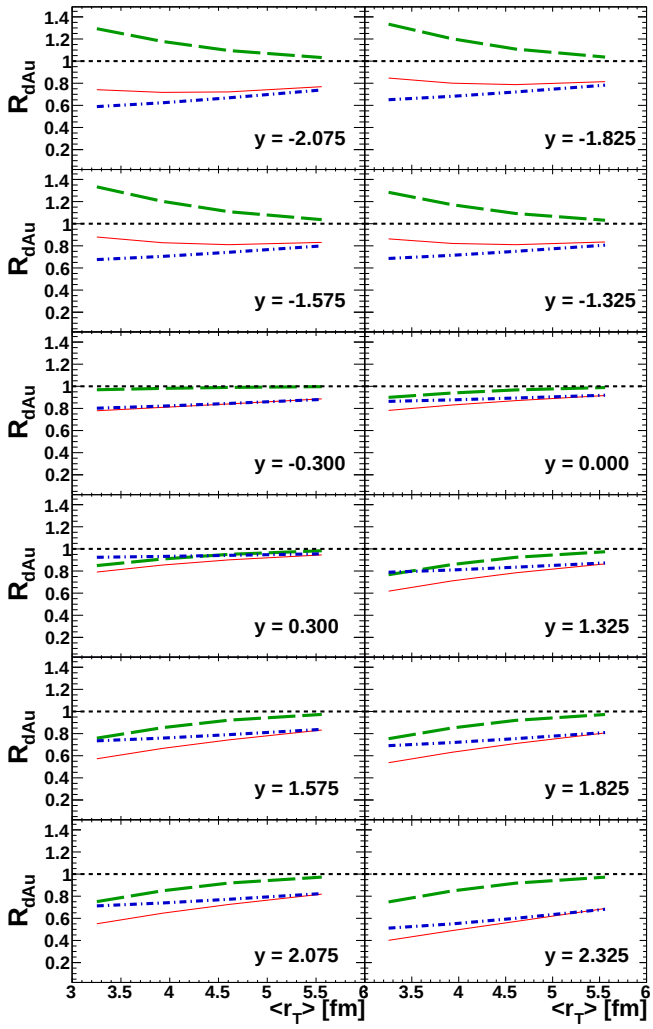

FIG. 6: (Color online) The nuclear modifications averaged over the PHENIX centrality resolution. The modification calculated from the fitted $\sigma_{\rm abs}$ alone is shown by the blue dot-dashed curve. The modification due to shadowing, calculated with Eq. (6) using the best fit global values of R and d, is shown by the green dashed curve. The product of the two effects, the overall calculated nuclear modification, is shown as the red solid curve.

B. Effective absorption cross section

The $\sigma_{\rm abs}$ values obtained from fits employing different assumptions for the centrality dependence of shadowing are all compared in Fig. 3. The fitted values of $\sigma_{\rm abs}$ are well defined and are essentially independent of the r_T dependence assumed for the shadowing prescription, suggesting that the effects of shadowing can be separated from those of physics processes that contribute to the value of the effective absorption cross section extracted for the $c\bar{c}$ pair. For specificity, in the following discussion we use the $\sigma_{\rm abs}$ values found using Eq. (6) with the values of R and d obtained from the global fit.

In practice, the effective absorption cross section encapsulates any physical process that reduces the J/ψ yield with an approximately exponential dependence on nuclear thickness. A mechanism that is linear in the nuclear thickness would be indistinguishable from exponential in this study and would contribute to $\sigma_{\rm abs}$. Thus $\sigma_{\rm abs}$ must contain a contribution from the reduction in J/ψ yield caused by the breakup of bound $c\bar{c}$ pairs in collisions with Au nucleons that pass through the production point after the hard scattering. Additionally, it would likely contain the effects of energy loss, resulting in an effective rapidity shift [17, 18].

A number of authors have pointed out that the $c\bar{c}$-nucleon cross section is expected to depend strongly on the size of the $c\bar{c}$ pair as it expands to a fully formed meson [19–22]. Therefore the proper time (in the frame of the $c\bar{c}$) over which the pair can collide with target nucleons should have an effect on the apparent magnitude of the absorption cross section. The asymptotic cross section should be independent of time. Figure 7 shows the values of $\sigma_{\rm abs}$ extracted from the PHENIX data as a function of the proper time spent by the $c\bar{c}$ in the target nucleus

$$\tau = \frac{\beta_z L}{\gamma} \ , \qquad (7)$$

where L is half of the target thickness, averaged over all impact parameters, and β_z is the longitudinal velocity of the $c\bar{c}$ relative to the target nucleus. The Lorentz factor γ for the $c\bar{c}$ in the frame of the target nucleus converts the nuclear crossing time into the proper time for the $c\bar{c}$. The measured mean transverse momentum, $\langle p_T \rangle$, was used when calculating γ at each rapidity. The value of L for a gold nucleus was taken from the Glauber model used in this work. The observed J/ψ yield includes feed-down from higher charmonium states. Following [22] we assume that the intermediate $c\bar{c}$ and all charmonia states have an average mass of 3.4 GeV/c^2 when calculating τ.

The data display different behaviors as a function of τ. Thus, in the next two subsections, we discuss the regions $\tau > 0.02$ fm/c (higher τ) and $\tau < 0.02$ fm/c (lower τ) separately.

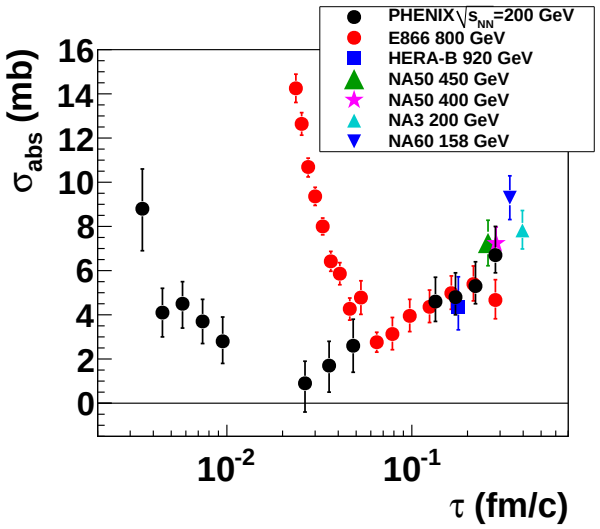

FIG. 7: (Color online) The effective $c\bar{c}$ absorption cross section $\sigma_{\rm abs}$ as a function of the proper time spent in the nucleus, τ. The times are extracted fom experiments over a range of energies. Those from the PHENIX $\sqrt{s_{NN}}$ = 200 GeV d+Au data were obtained after correcting for shadowing using the EPS09 NLO parameterization (this work). The values extracted from fixed target experiments were corrected for shadowing using the EKS98 parameterization. The fixed target $p+A$ data used in in Ref. [12] were from E866 at 800 GeV [23]; HERA-B at 920 GeV [24]; NA50 at 400 GeV [25] and 450 GeV [26]; and NA3 at 200 GeV [27]. Those for NA60 at 158 GeV were extracted in [28].

1. *Higher τ region*

It is notable that the mid and backward rapidity values of $\sigma_{\rm abs}$ extracted from the PHENIX data increase as τ increases from 0.02 fm/c to 0.3 fm/c, which is approximately the time scale over which a color singlet $c\bar{c}$ expands to its final size [22]. This is suggestive of the expected increase in $\sigma_{\rm abs}$ with time spent in the nucleus. On the other hand, the values of $\sigma_{\rm abs}$ begin to increase again as τ drops below ~ 0.01 fm/c. Since the $c\bar{c}$ formation time is expected to be ~ 0.05 fm/c [22], this increase of $\sigma_{\rm abs}$ with decreasing τ (increasing rapidity) is presumably of a different physical origin.

If the behavior of $\sigma_{\rm abs}$ at larger values of τ is dominated by the time the $c\bar{c}$ spends in the nucleus, then the τ dependence should be independent of center-of-mass energy.

Values of $\sigma_{\rm abs}$ have been extracted from fixed target data, after correcting for shadowing, at six energies in the range $\sqrt{s_{NN}} = 17.3 - 41.6$ GeV [12, 28, 29]. To be able to compare those $\sigma_{\rm abs}$ values to our results, it was necessary to estimate the average τ value in all six cases. That in turn requires an estimate of the $\langle p_T \rangle$ values. For HERA-B data at 920 GeV beam energy there is a parameterization of the p_T distribution [24] that provides values of both $\langle p_T \rangle$ and $\langle p_T^2 \rangle$. Additionally, that paper contains a systematic comparison of data from collisions at beam energies of 450 GeV, 800 GeV and 920 GeV showing that $\langle p_T^2 \rangle$ is linear with the square of the collision energy. Using that fact, and assuming that the ratio $\langle p_T \rangle / \sqrt{\langle p_T^2 \rangle}$ is approximately constant from $\sqrt{s_{NN}} = 17.3 - 41.6$, we were able to estimate the values of $\langle p_T \rangle$, and thus τ, at all six energies.

We have added to Fig. 7 the values of $\sigma_{\rm abs}$ extracted in [12] from fixed target $p+A$ data from E866 at 800 GeV; HERA-B at 920 GeV; NA50 at 450 and 400 GeV; and NA3 at 200 GeV. The latter four values were extracted at y=0, while the E866 data cover a wide range of rapidities. In all cases the data were corrected for shadowing using the EKS98 parameterization. The error bars shown include systematic uncertainties. We consider those cross sections to be directly comparable to the $\sigma_{\rm abs}$ values extracted here using EPS09 shadowing, since the EKS98 and EPS09 central gluon modifications are very similar [5]. We have also included the $\sigma_{\rm abs}$ value extracted from the NA60 data for $y \sim 0.3$ at 158 GeV [28, 29], where shadowing was also corrected for using the EKS98 parameterization.

TABLE I: Kinematic characteristics used to determine the average time, τ, the J/ψ spends in the nucleus for several experiments and targets, shown in Fig. 7.

Exp.	$\sqrt{s_{NN}}$ (GeV)	A	$y_{\rm beam}$	$y_{\rm cm}$	L (fm)	$\langle p_T \rangle$ GeV/c	τ (fm/c)
PHENIX	200	Au	5.36	-2.08-2.32	4.36	1.90	0.283-0.0035
HERA-B	41.6	W	7.58	0.0	4.26	1.36	0.178
E866	38.8	W	7.44	-0.39-2.1	4.26	1.32	0.283-0.024
NA50	29.1	W	6.87	0.0	4.26	1.22	0.258
NA50	27.4	Pb	6.75	0.0	4.44	1.20	0.286
NA3	19.4	Pt	6.06	0.0	4.34	1.14	0.396
NA60	17.3	Pb	5.82	0.3	4.44	1.12	0.339

The average L, $\langle p_T \rangle$ and the kinematics characteristic of the experiments used to calculate the τ values from Eq. (7), displayed in Fig. 7, are given in Table I. The W/Be ratios were used for E866; W/C ratios for HERA-B; and Pt/H ratios for NA3. A range of targets was employed by the NA50 and NA60 Collaborations, and the value of L for the heaviest target is shown in Table I. The L values for all targets other than Au were obtained from the Au value assuming $A^{1/3}$ scaling.

For τ greater than 0.05 fm/c the lower energy data seem to follow the same trend as those extracted from PHENIX data. The data in Fig. 7 cover the energy range $17.3 \leq \sqrt{s_{NN}} \leq 200$ GeV. The common behavior of $\sigma_{\rm abs}$ with τ for $\tau > 0.05$ fm/c across such a large $\sqrt{s_{NN}}$ range is striking.

The results in Fig. 7 imply that, for $\tau > 0.05$ fm/c, $\sigma_{\rm abs}$ depends on the time the $c\bar{c}$ spends in the nucleus. Thus $\sigma_{\rm abs}$ is a function of both the nuclear target mass and impact parameter. This was not taken into account when extracting the values of $\sigma_{\rm abs}$ included in Fig. 7. However,

we note that changing the average L by a factor of two produces only about a 1 mb change in $\sigma_{\rm abs}$. Therefore averaging $\sigma_{\rm abs}$ over a range of impact parameters and, in the case of the NA50 400 and 450 GeV data, over a range of targets, may be acceptable.

A description of charmonium suppression by nucleon absorption in p+A collisions proposed by Arleo *et al.* [22] may be illustrative in this large τ region. In this approach, the $c\bar{c}$ pair, assumed to be initially formed in a color octet state, neutralizes its color by gluon emission and expands to the physical size of the meson. In cases where τ is short, the $c\bar{c}$ travels through the target as a colored object. When τ is long, it travels through the target as an expanding or fully-formed color singlet. In the latter case, the absorption cross section depends on τ due to the dependence of the $c\bar{c}$ radius on τ.

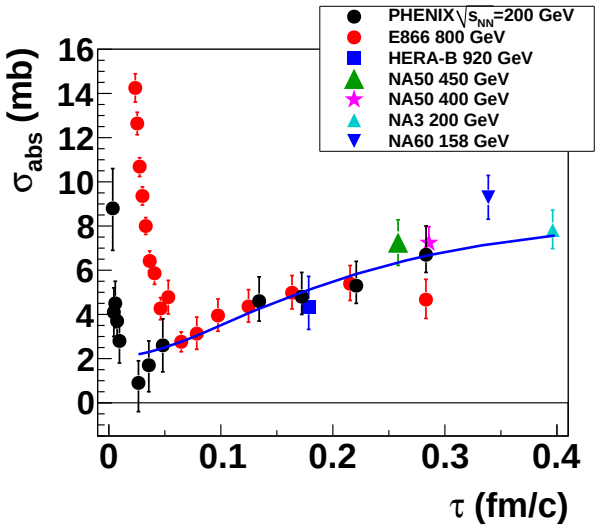

FIG. 8: (Color online) The same data as in Fig. 7 plotted on a linear scale compared to a calculation of the cross section based on the model of Ref. [22].

When the $c\bar{c}$ is still expanding, the τ dependence of $\sigma_{\rm abs}$ was assumed to be [22]

$$\sigma_{\rm abs}(\tau) = \sigma_1 \left(\frac{\sqrt{s}}{10\ {\rm GeV}} \right)^{0.4} \left(\frac{r_{c\bar{c}}(\tau)}{r_{{\rm J}/\psi}} \right)^2 , \qquad (8)$$

where σ_1 is the cross section for destruction of a fully formed J/ψ in an interaction with a nucleon at $\sqrt{s} = 10$ GeV. The time dependence of the $c\bar{c}$ radius was taken to be

$$r(\tau) = r_0 + v_{c\bar{c}}\tau \ \ ({\rm if}\ r(\tau) < r_\psi)\ . \qquad (9)$$

In Ref. [22] it was assumed that the observed J/ψ yield was a combination of direct J/ψ production and feed down from the ψ' and χ_c. The model parameters were extracted from fits to the A dependence of the E866 J/ψ data. However, no correction was made for shadowing. Thus the parameters obtained in Ref. [22] are not appropriate for the shadowing-corrected $\sigma_{\rm abs}$ values we extract from the PHENIX data, or the shadowing corrected $\sigma_{\rm abs}$ values extracted from the lower energy data. Therefore we have fitted the parameters in Eqs. (8) and (9) to the subset of the cross section data shown in Fig. 7 with $\tau > 0.05$ fm/c ($\tau > 0.02$ fm/c for PHENIX). At each energy and rapidity, the calculated $\sigma_{\rm abs}$ was averaged over r_T using the distribution of nucleon-nucleon collisions obtained from the Glauber simulation, and averaged over the (longitudinal) z dimension using the same Woods Saxon distribution as was used in the Glauber simulation.

Because the data being fitted are from a variety of targets and a wide range of collision energies, we have made some simplifying approximations. First, we calculated the τ values only for the $\langle p_T \rangle$ at each energy (see Table I), rather than averaged over the p_T distribution. This assumption was checked for the PHENIX 200 GeV case by averaging over the full measured p_T distribution in the Glauber model, and it was found to give the same result for the average τ and average $\sigma_{\rm abs}$ to much better than 1%. Second, we assumed that the distribution of nucleon-nucleon collisions for all targets (mass range 184 to 208) was adequately described by that for Au (mass 197). For the lower energy data, the average τ values obtained using this assumption differed by less than 2.5% from those obtained using the $A^{1/3}$ scaled average length given in Table I.

The fraction of J/ψ's arising from direct production together with ψ' and χ_c feed down were taken to be 58%, 10% and 32% respectively, see Ref. [30]. The radii of the three $c\bar{c}$ states were assumed to be 0.43 fm for the J/ψ, 0.87 fm for the ψ' and 0.67 fm for the χ_c, as in Ref. [22].

The best fit of Eqs. (8) and (9) to the high τ data is shown in Fig. 8. The optimum values of the parameters are $\sigma_1 = 7.2$ mb, $r_0 = 0.16$ fm and $v_{c\bar{c}} = 1.0$. The curve resulting from the fit describes all of the high τ $\sigma_{\rm abs}$ values very well, with a χ^2/dof of 0.94. We note that the fitted value of σ_1 is considerably larger than that obtained in Ref. [22]. The difference arises, at least in part, due to the substantial antishadowing correction from the EPS09 and EKS98 parameterizations used to extract the $\sigma_{\rm abs}$ values from data at higher τ, which results in larger $\sigma_{\rm abs}$ than those extracted from fits without any shadowing correction [12].

The collision energy dependence of $\sigma_{\rm abs}$ at $y = 0$ obtained from the fit shown in Fig. 8 is compared with data in Fig. 9.

We conclude that a model of time-dependent nucleon absorption such as that of Ref. [22] is capable of describing the trend of the $\sigma_{\rm abs}$ values extracted from the PHENIX data at mid- and backward rapidity, as well as those extracted from lower energy data for $\tau > 0.05$ fm/c.

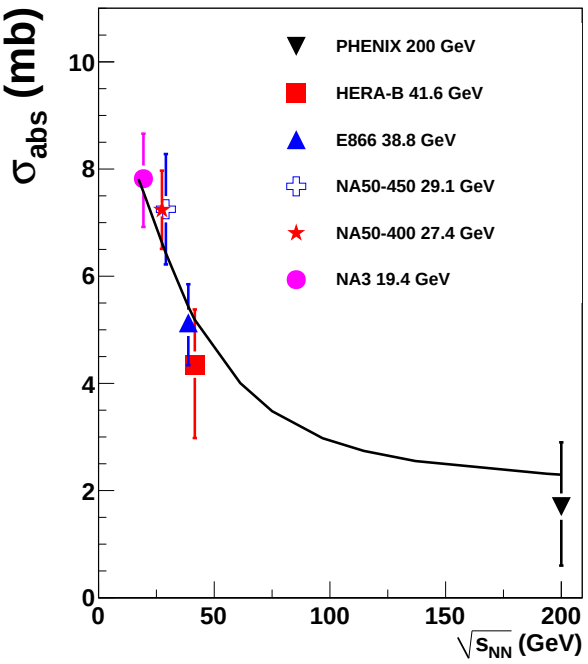

FIG. 9: (Color online) Measured $\sigma_{\rm abs}$ values at $y = 0$ compared with the energy dependence calculated from the best fit to $\sigma_{\rm abs}$ versus τ shown in Fig. 8. The 200 GeV data point is from the present work, all others are from [12].

2. *Lower τ region*

The other striking feature of the τ dependence of $\sigma_{\rm abs}$ is the departure from τ scaling when the $c\bar{c}$ spends only a short time traversing the nucleus. The results extracted from the PHENIX and E866 data both show a strong increase in $\sigma_{\rm abs}$ at small τ, starting at $\tau \sim 0.05$ fm/c in the E866 case and at $\tau \sim 0.02$ fm/c for PHENIX. These times are smaller than or comparable to the $c\bar{c}$ formation time and the color neutralization time. Several models have been proposed which might explain increased J/ψ suppression at forward rapidity.

Arleo *et al.* [22] assumed that the increased E866 cross section at forward x_F (rapidity) was due to the interaction of nucleons with the color octet state. Here the τ-independent cross section is $22.3(\sqrt{s_{NN}}/10)^{0.4}$ mb for $\tau < 0.02$ fm/c, the color neutralization time, a parameter of their model. Such behavior leads to increasing suppression with decreasing τ because a smaller fraction of $c\bar{c}$ pairs escape before the color neutralization time is reached. In this picture, the increased suppression at forward rapidity is due to breakup by nucleons. However, in this approach, $\sigma_{\rm abs}$ should also scale with τ which clearly does not hold for the E866 and PHENIX data at small τ, as seen in Fig. 7. Therefore, other mechanisms need to be considered.

In a recent paper, Arleo and Peigne [18, 31] describe forward rapidity data from NA3, E866 and PHENIX using a model of parton energy loss in cold nuclear matter. The $c\bar{c}$ pair is assumed to be in an essentially point-like long-lived color octet state, $\tau_{\rm octet} \gg \tau_{c\bar{c}}$, where $\tau_{c\bar{c}} \sim 1/M$, the inverse of the pair mass, with a lifetime less than that of the formation time of the J/ψ. In this picture, gluon splitting, $g \to Q\overline{Q}$, is followed by scattering with a gluon in the target nucleus. The scattering with the target gluon is similar to Bethe-Heitler radiation off a fast color octet undergoing transverse momentum broadening by scattering with a coherent color field. Since the scattering is from a target gluon, Drell-Yan production, quarkonium photoproduction and nDIS are unaffected by this radiation. They find $\Delta E \propto E$, as in Refs. [32, 33], in contradiction to the energy independent bound derived in Ref. [34] which neglected nuclear broadening in the final state. Arleo and Peigne suggest that the bound holds only for abelian models and not in the non-abelian case of QCD. They fit the energy loss parameter $\hat{q}$ to the E866 J/ψ data as a function of x_F and use that same parameter to calculate results at different energies. They assume $2 \to 1$ kinematics and fit the pp production cross section to a power law in x, $d\sigma_{pp}/dx_F \propto (1-x)^n/x$ rather than making any assumptions about the quarkonium production mechanism. Since the parameter governing energy loss is related to the transverse momentum broadening of the state, $l_T^2 \simeq \hat{q}L$, there is some centrality dependence that can be introduced into the model in future work.

Arleo and Peigne added suppression of the J/ψ yield by either gluon saturation or standard shadowing parameterizations, including EPS09. They did not, however, incorporate nuclear absorption, which they noted may become important at backward rapidity. Adding EPS09 shadowing led to very good agreement with the PHENIX $R_{\rm dAu}$ data at forward rapidity and midrapidity. However, it resulted in a considerable overprediction of the data (underpredicting the suppression) at backward rapidity. Their backward rapidity result seems to be consistent with our present results, where we find evidence that at backward rapidity the modification is well described by a large absorption cross section together with antishadowing.

Thus in the small τ (forward rapidity) region, energy loss effects may explain the rise in the effective absorption cross section observed here. If that is the case, the large effective absorption cross section we obtain at small τ is not due to $c\bar{c}$ breakup, but is rather an energy loss-induced shift in the rapidity of the detected J/ψ. The effect is expected to depend on the square root of the thickness [31], rather than the exponential dependence implied by our use of an effective absorption cross section. However the $\sqrt{T_A}$ dependence is sufficiently close to exponential that our fitting procedure is unable to discriminate between them.

C. Shadowing

The gluon modification obtained from the EPS09 NLO parameterization using Eq. (6), with global fit values of R and d as a function of r_T, is shown by the solid red line in Fig. 10. The effect of the combined uncertainty in R and d can be visualized by plotting the modifications for all combinations of R and d that produce a $\overline{\chi}^2$ value inside the $\Delta\overline{\chi}^2 = 2.3$ contour [35] (see Fig. 4). These are represented by the thin blue lines in Fig. 10. In all cases, the calculated modification is significant only for $r_T \lesssim 3$ fm. Therefore, we conclude that the data constrain the nuclear modification to be important only at small r_T. The modification obtained with the best fit global power, $T_A^n(r_T)$, $n = 15$, is shown as the dotted orange line in Fig. 10. Although there is some difference in the details at small r_T, albeit within the uncertainties, the two prescriptions give essentially the same values of $\overline{\chi}^2$/dof. Thus the data appear to be insensitive to the detailed shape of the modification at low r_T. This is because the d+Au centrality bins are wide and significantly overlap. If the centrality bins were narrower, the sensitivity to the centrality dependence could be increased.

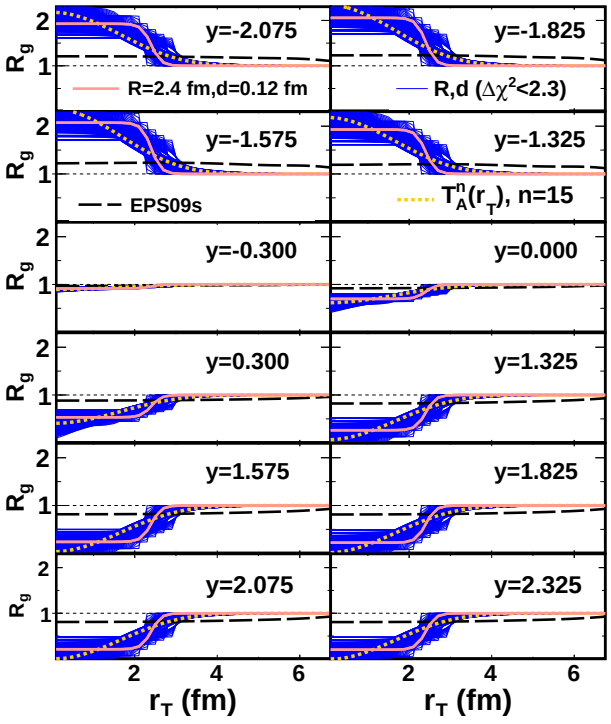

FIG. 10: (Color online) The gluon modification from the best fit global R and d parameters (solid red line), along with the modifications from all combinations of R and d that fall within the $\Delta\overline{\chi}^2 = 2.3$ contour in Fig. 4 (thin blue lines). The modification from the best fit global analysis of $T_A^n(r_T)$ ($n = 15$) is shown by the dotted orange line. The dashed black line is the recently released EPS09s NLO impact parameter dependence [9].

We compare our results obtained from the fits to the J/ψ data with those given by the newly-available impact parameter dependent EPS09s (NLO) set [9], shown by the dashed black line in Fig. 10. The EPS09s result has a much weaker dependence on r_T than obtained from our fits. A study of the target mass systematics of J/ψ production in d+A collisions at RHIC may shed light on the source of this pronounced difference.

D. Effect of nonlinear shadowing on $\sigma_{\rm abs}$

In Fig. 7 we compare the $\sigma_{\rm abs}$ values extracted from the PHENIX data in this work with the $\sigma_{\rm abs}$ values extracted from centrality-integrated lower energy data [12] or, for NA60 p+Pb, from fits to centrality-dependent data [28] that assumed a linear dependence of shadowing on nuclear thickness. Thus when comparing our values of $\sigma_{\rm abs}$ with those obtained at lower energy, it is important to understand if the $\sigma_{\rm abs}$ values extracted from PHENIX data here depend strongly on the centrality dependence assumed for the shadowing.

Fig. 11 compares the $\sigma_{\rm abs}$ values extracted from the PHENIX data using Eq. (6) with global values of R and d, the values used in Fig. 7, with $\sigma_{\rm abs}$ values extracted assuming a linear dependence of shadowing on nuclear thickness. While there are some differences in the extracted $\sigma_{\rm abs}$ if the shadowing has a linear thickness dependence, they are not large enough to affect the conclusions drawn from Fig. 7.

We emphasize that the shadowing description of the PHENIX data at both backward and forward rapidity is much poorer when a linear thickness dependence is assumed. At the four backward rapidities, the $\overline{\chi}^2$ worsens by 4.3, while at the five forward rapidities it worsens by 47.6. At midrapidity, where the shadowing is weak, the $\overline{\chi}^2$ worsens by only 0.8.

V. SUMMARY AND CONCLUSIONS

In summary, we have fitted the centrality and rapidity dependent PHENIX $\sqrt{s_{NN}} = 200$ GeV d+Au J/ψ data with Glauber calculations employing an effective absorption cross section, $\sigma_{\rm abs}$, with several prescriptions for the impact parameter dependence of the EPS09 NLO central gluon shadowing parameterization. The fits properly account for all of the experimental systematic uncertainties. We find little ambiguity between $\sigma_{\rm abs}$ and the functional form of the centrality dependence of shadowing.

The values of $\sigma_{\rm abs}$ exhibit a characteristic rapidity dependence, with a minimum at midrapidity. When plotted as a function of the average time the $c\overline{c}$ spends in the nucleus, τ, the $\sigma_{\rm abs}$ values extracted from the PHENIX data at $\sqrt{s_{NN}} = 200$ GeV and from lower energy data with $17.3 < \sqrt{s_{NN}} < 41.6$ GeV, display a common τ dependence for $\tau > 0.05$ fm/c. In that τ range the cross section is very well described when the data are fitted

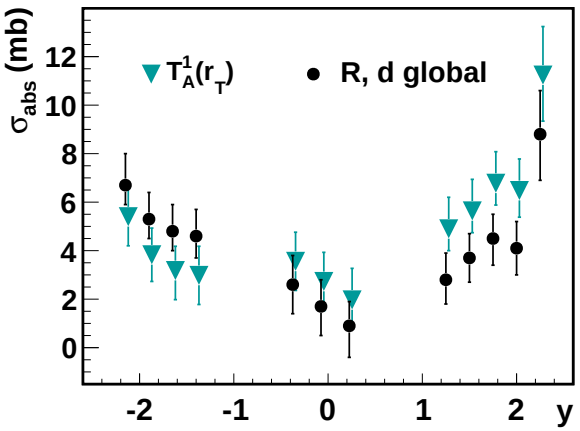

FIG. 11: (Color online) Comparison of the $\sigma_{\rm abs}$ values extracted from the PHENIX data assuming a linear thickness dependence for the shadowing with those extracted using Eq. (6) assuming global values of R and d.

with a model in which the $c\bar{c}$-nucleon cross section depends on the size of a color neutral $c\bar{c}$ as it expands into a fully-formed meson. Such a model naturally leads to scaling of $\sigma_{\rm abs}$ with τ. The best fit parameters provide an excellent description of the collision energy dependence of $\sigma_{\rm abs}$ at $y = 0$ from $\sqrt{s_{_{NN}}} = 20 - 200$ GeV.

As τ decreases below $\sim$ 0.02 fm/c, the $\sigma_{\rm abs}$ values extracted from the PHENIX data rise sharply. This τ range is smaller than the expected $c\bar{c}$ formation time and color neutralization time, and reflects different physical processes than those active at higher τ. The $\sigma_{\rm abs}$ values extracted from E866 data at $\sqrt{s_{_{NN}}} = 41.6$ GeV also exhibit a sharp rise beginning at $\tau \sim 0.05$ fm/c. The PHENIX and E866 data show no scaling with τ in the range $\tau < 0.05$ fm/c. The present results at low τ (forward rapidity) seem to be consistent with energy loss of a color octet $c\bar{c}$ state in cold nuclear matter [18, 31]. If so, the fitted effective $\sigma_{\rm abs}$ values do not reflect breakup of the $c\bar{c}$ pairs, but instead an energy-loss induced rapidity shift of the J/ψ.

The centrality dependence of shadowing extracted from the data turns on sharply for $r_T \leq 3$ fm, in significant disagreement with the weaker r_T dependence of EPS09s NLO. Indeed, the EPS09s dependence is somewhat weaker than the linear dependence on the thickness function assumed in Ref. [6]. A study of the target mass systematics of J/ψ production in d+A collisions at RHIC may shed light on the source of this pronounced difference.

While we have employed only the central EPS09 set in our calculations, using all 31 EPS09 sets would not affect our overall conclusions regarding the sharp turn on of shadowing with r_T, only increase the uncertainty in the value of $\sigma_{\rm abs}$ as a function of rapidity. The use of alternative nPDF sets [2-5] would also change $\sigma_{\rm abs}(y)$ without affecting the r_T dependence of shadowing. The strong impact parameter dependence suggested here seems to be in accord with the 'hot spots' conjectured in a saturated medium of high gluon density. Such behavior at backward rapidity, in the antishadowing region, is, however, at odds with the saturation picture and may more simply suggest that shadowing effects are concentrated in the core of the nucleus instead of throughout the nuclear volume.

Acknowledgments

The work of R. V. was performed under the auspices of the U.S. Department of Energy by Lawrence Livermore National Laboratory under Contract DE-AC52-07NA27344, and supported in part by the JET collaboration. The work of A.D.F and D.C.M. was supported in part by the National Science Foundation grant number PHY-10-64819.

[1] F. Gelis, E. Iancu, J. Jalilian-Marian, and R. Venugopalan, Ann. Rev. Nucl. Part. Sci. **60**, 463 (2010).
[2] M. Hirai, S. Kumano, and T. H. Nagai, Phys. Rev. C **76**, 065207 (2007).
[3] K. Kovarik *et al.*, Phys. Rev. Lett. **106**, 122301 (2011).
[4] D. de Florian, R. Sassot, P. Zurita, and M. Stratmann, Phys. Rev. D **85**, 074028 (2012).
[5] K. J. Eskola, H. Paukkunen, and C. A. Salgado, JHEP **0904**, 065 (2009).
[6] S. R. Klein and R. Vogt, Phys. Rev. Lett. **91**, 142301 (2003).
[7] L. Frankfurt, V. Guzey, and M. Strikman, Phys. Rev. D **71**, 054001 (2005).
[8] K. J. Eskola, V. J. Kolhinen, and C. A. Salgado, Eur. Phys. J. C **9**, 61 (1999).
[9] I. Helenius, K. J. Eskola, H. Honkanen, and C. A. Salgado (2012), 1205.5359.
[10] A. Adare *et al.*, Phys. Rev. Lett. **107**, 142301 (2011).
[11] J. L. Nagle, A. D. Frawley, L. A. Linden Levy, and M. G. Wysocki, Phys. Rev. C **84**, 044911 (2011).
[12] C. Lourenço, R. Vogt, and H. K. Wöhri, JHEP **02**, 014 (2009).
[13] M. L. Miller, K. Reygers, S. J. Sanders, and P. Steinberg, Ann. Rev. Nucl. Part. Sci. **57**, 205 (2007).
[14] A. Adare *et al.* (2012), 1204.0777.
[15] R. Gavai *et al.*, Int. J. Mod. Phys. A **10**, 3043 (1995).
[16] A. Adare *et al.*, Phys. Rev. C **77**, 064907 (2008).
[17] D. Kharzeev and H. Satz, Z. Phys. C **60**, 389 (1993).
[18] F. Arleo and S. Peigne (2012), 1212.0434.
[19] G. Farrar, L. Frankfurt, M. Strikman, and H. Liu, Phys. Rev. Lett. **64**, 2996 (1990).
[20] J. Blaizot and J.-Y. Ollitrault, Phys. Lett. B **217**, 386 (1989).
[21] S. Gavin and R. Vogt, Nucl. Phys. B **345**, 104 (1990).

[22] F. Arleo, P. Gossiaux, T. Gousset, and J. Aichelin, Phys. Rev. C **61**, 054906 (2000).
[23] M. Leitch *et al.* (FNAL E866/NuSea collaboration), Phys. Rev. Lett. **84**, 3256 (2000).
[24] I. Abt *et al.* (HERA-B Collaboration), Eur. Phys. J. C **60**, 525 (2009).
[25] B. Alessandro *et al.* (NA50 Collaboration), Eur. Phys. J. **C48**, 329 (2006).
[26] B. Alessandro *et al.* (NA50 Collaboration), Eur. Phys. J. C **33**, 31 (2004).
[27] J. Badier *et al.* (NA3 Collaboration), Z. Phys. C **20**, 101 (1983).
[28] R. Arnaldi *et al.* (NA60 Collaboration), Phys. Lett. B **706**, 263 (2012).
[29] R. Arnaldi (NA60 Collaboration), Nucl. Phys. A **830**, 345C (2009).
[30] A. Adare *et al.* (PHENIX Collaboration), Phys. Rev. D **85**, 092004 (2012).
[31] F. Arleo and S. Peigne, Phys. Rev. Lett. **109**, 122301 (2012).
[32] S. Gavin and J. Milana, Phys. Rev. Lett. **68**, 1834 (1992).
[33] M. Johnson, B. Kopeliovich, I. Potashnikova, P. McGaughey, J. Moss, *et al.*, Phys. Rev. C **65**, 025203 (2002).
[34] S. J. Brodsky and P. Hoyer, Phys. Lett. B **298**, 165 (1993).
[35] W. H. Press, S. A. Teukolsky, W. T. Vetterling, and B. P. Flannery, *Numerical Recipes in C: The Art of Scientific Computing* (Cambridge University Press, 1993).